Solid State Phenomena
ISSN: 1662-9779, Vol. 389, pp 1-9
doi:10.4028/p-u5oc0K

Submitted: 2025-12-19
Revised: 2026-02-23
Accepted: 2026-02-24
Online: 2026-04-16

Hot Double-Sided Incremental Forming of Fiber-Reinforced Thermoplastics: Process Capabilities and Challenges

Jan-Erik Rath[1,a*], Doran Nettig[1,b] and Thorsten Schüppstuhl[1,c]

[1]Hamburg University of Technology, Institute of Aircraft Production Technology, Denickestr. 17, 21073 Hamburg, Germany

[a*]jan-erik.rath@tuhh.de, [b]doran.nettig@tuhh.de, [c]schueppstuhl@tuhh.de

[*]corresponding author

Keywords: incremental sheet forming, composite, fiber reinforced plastic, free forming, robot.

Abstract. Fiber-reinforced thermoplastics (FRTP) offer high strength-to-weight ratios as well as weldability and recyclability, making them attractive for lightweight applications. Conventional thermoforming of continuous FRTP, however, requires part-specific molds, limiting economic viability for prototypes, individual parts, and small series. This study investigates a robotic hot double-sided incremental forming (DSIF) process developed for dieless, flexible forming of continuous FRTP sheets together with metal dummy sheets. Five different generic demonstrator parts with varying wall angles, degrees of symmetry, forming depths, and sizes were formed to assess process capability. Results demonstrate that typical defects such as fabric wrinkling and deconsolidation can be successfully avoided, and that the geometric accuracy achievable is comparable to that of metal DSIF. Challenges exist in forming larger parts due to the failure of the employed metal dummy sheets.

Introduction

The utilization of fiber-reinforced plastics (FRPs) in high-performance applications across aerospace, automotive, sports, and medical sectors continues to show significant growth [1]. Among the various reinforcement architectures, woven fabrics made from glass and carbon fiber are common as they offer a good compromise of mechanical reinforcement, handling properties, and drapability, alongside broad availability [2]. Compared to traditional thermosets, thermoplastic matrices are increasingly preferred, attributed to their enhanced ductility, damage tolerance, and inherent capabilities for welding, reshaping, and recycling [1,3]. The high viscosity of thermoplastics favors the use of fully impregnated and consolidated organosheets as semi-finished products. These are formed using thermoforming techniques that require part-specific molds, which are associated with significant tooling costs and long lead times until the first part is produced. Thus, prototype, individual part, and small-scale production are, in many cases, uneconomical [4,5].

Incremental sheet forming (ISF) could be a flexible, dieless manufacturing alternative. In this process, a simple standard tool traverses a numerically controlled trajectory, locally deforming a clamped sheet material [6]. Variants of ISF include single-point (SPIF), two-point (TPIF), and double-sided incremental forming (DSIF), with DSIF emerging as the most promising configuration in terms of achievable formability, flexibility, and geometric accuracy [7,8]. While ISF is well-established for metals and partially adapted for thermoplastics [9,10], its transfer to continuous fiber-reinforced thermoplastic (FRTP) composites is associated with some unique challenges and is still at an early stage of research [5,11].

The anisotropic, inextensible nature of continuous woven fibers in FRTPs requires fabric draping governed by bending, in-plane shear, and intra-ply sliding as deformation mechanisms, rather than the stretch-dominated modes prevalent in metals and polymers [12,13]. Consequently, rigid clamping of the organosheet is not possible without fiber breakage [11]. Therefore, researchers such as Al Obaidi et al. [5] adopted a “floating” clamping configuration, in which the organosheet is interposed between two metallic dummy sheets, separated by PTFE sheets, allowing relative movement during SPIF. During the process, the thermoplastic matrix must be heated to above its glass-transition or

melting temperature to allow formability, which was realized by clamping the sheet layup on top of an isolated chamber heated by hot air blowers [5,14], a thermal radiation plate [11], or an infrared lamp [15,16]. Also, the utilization of a heated and pressurized fluid was proposed [17]. Most of those SPIF approaches employed elementary z-level or spiral toolpath strategies known from metal ISF, not considering the draping behavior of FRTP. Consequently, defects such as wrinkling, cracking, and delamination occurred, and forming depth and wall angles were limited [5,11,15,16]. Drape-aware SPIF toolpaths proposed by Rath and Schüppstuhl [14] have shown promise in suppressing wrinkling and enhancing dimensional accuracy. However, the separation of the metal dummy sheets due to unwanted global deformation remained problematic when the distance between the clamped edge and the formed geometry was high in the SPIF process [14].

Therefore, the authors developed and successfully implemented the first DSIF system tailored to the forming of FRTP, offering a force-controlled flexible local support on the back side of the layup [18]. This setup, employing two synchronized industrial robots, is briefly described in the next section. Forming experiments are conducted with woven fiber reinforced organosheets, producing five different demonstrator parts, one of which in three different sizes. Results are analyzed qualitatively for wrinkling and deconsolidation defects, and geometric accuracy is quantified.

Materials and Methods

Hot DSIF Setup.

The setup for hot DSIF of FRTPs is depicted in Fig. 1 and described in detail in [18]. It relies on two KUKA KR 300 industrial robots with handling capacities of 300 kg, mounted on a steel platform on opposing sides of a modular clamping frame. The frame carries a stainless-steel base plate which is designed to secure either sheet layups of 695 x 695 mm² or a reduction module for sheet layups of 350 x 350 mm² with toggle clamps. The layups, in which the FRTP is quasi-floatingly interposed between two metal dummy sheets, are prepared on a separate layup table and clamped via peripheral clamping strips with screws. After securing a clamped layup on the base plate or the reduction module, the sheets are heated globally by a PID-controlled closed convective oven system. While the layup and base plate constitute one side of the oven, the other is comprised of a flexible insulation material suspended between the base plate and the flange of the support robot, allowing the necessary tool movement within the enclosed hot area. A water-cooled cooling coupler decouples the six-axis force-torque measurement cell (Schunk FTN-Omega 160) mounted on the robot flange from the hot side of the support tool. Tools with hemispherical tips and different diameters can be attached via a collet system. The main forming tool is designed similarly but employs a Schunk FTN-Omega 191 force-torque cell for higher loads and does not require cooling.

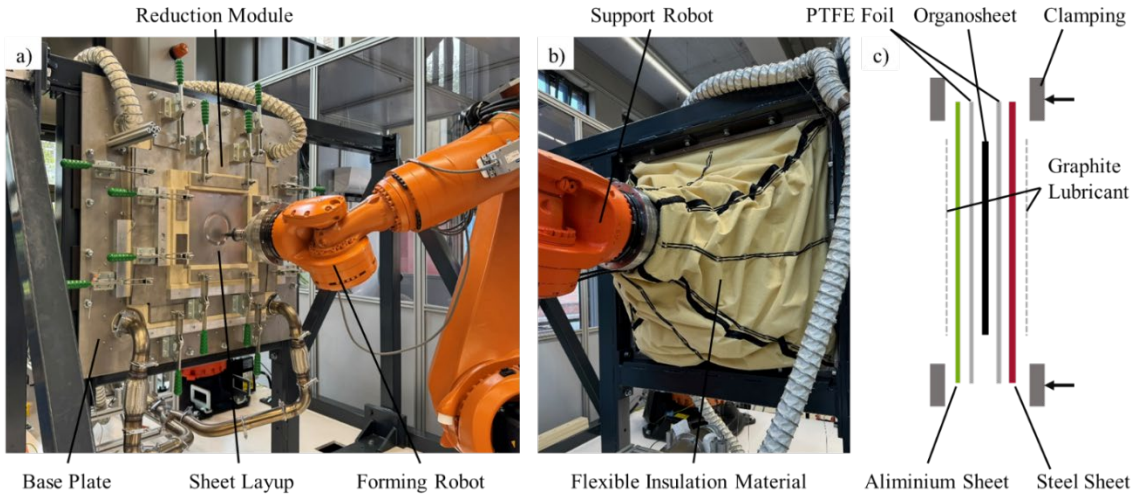

Fig. 1. Hot DSIF Setup for FRTP forming – a) front view with reduction module and clamped sheet layup, b) back view with flexible insulation material (right), c) illustration of sheet layup.

In operation, the robot carrying the main (guiding) forming tool is position-controlled and follows the programmed toolpath. The motion of the support robot is geometrically coupled to that of the guiding robot via KUKA RoboTeam. The time-synchronized relative-motion commands of the support robot are calculated as offsets from the center point of the main tool along the normal of the formed surface. To maintain the target normal force, an implicit PD-force controller continually adjusts the tool separation based on load-cell feedback [18].

Materials.

Styrene-acrylonitrile (SAN) organosheets with two layers of twill-woven carbon fibers with a basis weight of 245 g/m² and a resulting fiber-volume-content of 47 % at 0.6 mm thickness were cut to three different sizes: 200 x 200 mm², denoted as S, 300 x 300 mm² (M), and 615 x 615 mm² (L). Layups were prepared using DC04 steel sheets with a thickness of 0.7 mm on the front side and aluminum EN AW-1050A H111 sheets with a thickness of 1 mm on the back (supporting tool) side. Organosheet sizes S and M were interposed between metal sheets of 350 x 350 mm², and L between metal sheets of 695 x 695 mm². Fiber orientations were aligned with the sheet edges. PTFE sheets of 0.05 mm thickness and the same sizes as the metal dummy sheets were used to separate metal and organosheets and to allow the relative movement with a low coefficient of friction. To keep the organosheet in its central position, it was attached to the underlying PTFE sheet with polyimide tape in its corners. Graphite spray was applied to the outside faces of the metal dummy sheets to reduce friction with the tooltips. The layup is illustrated in Fig. 1 c).

Forming Experiments.

To investigate the capabilities of the process, five different demonstrator geometries, D1-D5, described in Table 1, were produced. In addition to a cone, which is a standard geometry commonly used in the ISF state of the art, four more complex geometries were designed to address various process challenges. These were multi-curved surface geometries that varied in terms of degree of symmetry, maximum wall angle, and minimum corner radius. In addition, one of the geometries was produced in three different sizes, S-L, to investigate the scalability of the process. The development of the applied processing strategy will be described in detail in a separate publication.

Table 1. Demonstrator geometries with geometric data.

Name	Description	Size	Depth	Wall Angle	Forming Strategy
D1-S	Cone	Ø 160 mm	40 mm	40°	S12-S12-S9-D3-S3-S0
D2-S	Cone with varying wall angle	Ø 160 mm	40 mm	max 60°	S12-S12-S9-D3-S3-S0
D2-M		Ø 220 mm	50 mm	max 60°	S12-S12-S9-S9-D3-S3-S0
D2-L		Ø 500 mm	70 mm	max 60°	S33-S30-D3-S3-S0
D3-S	Cone with eccentric tip	Ø 160 mm	25 mm	max 28.4°	S9-S9-D3-S3-S0
D4-S	Square pyramid with twisted circular tip	180 x 180 mm²	44 mm	35°	S12-S12-S12-D3-S3-S0
D5-S	Square pyramid with varying wall angle	160 x 160 mm²	50 mm	40-60°	S12-S15-S15-D3-S3-S0

After preparing, clamping, and securing the layup, the air inside the oven chamber was heated to the target temperature of 180 °C, measured with a type K thermocouple at mid-height next to the sheet layup. During heating, the clamping force was kept low to allow the thermal expansion of the metal sheets. After reaching the target temperature, the clamping force was increased. Forming was then conducted with hemispherical hardened steel 1.2210 tooltips with 20 mm diameter, while the temperature was maintained. The support force was set to 200 N and the tool speed to 20 mm/s.

Based on stl meshes of the target geometries, toolpaths were generated by a custom path planning digital process chain, which will be thoroughly described in another publication. In the first step, the target geometry is divided into multiple intermediate shapes using linear height interpolation to improve formability. The approximate maximum depth increase in each intermediate shape is noted next to the utilized toolpath strategy designation in Table 1. For each shape, toolpaths can be

generated according to two different strategies. The first is a spiral contour toolpath strategy, commonly used for metal ISF, with a constant scallop height of 2 mm. This toolpath strategy is denoted S in Table 1 and is depicted in Fig. 2 b). The second strategy is a refinement of the fiber-following draping strategy that showed promising results in suppressing wrinkles in the SPIF experiments in [14]. It builds upon an approximation of the fiber orientations in the target shape. Starting with two central orthogonal paths following the initial 0/90° fiber orientations, the shape is covered inside outwards in parallel lines with the same path distance of 2 mm, which are connected to a continuous path. This strategy, denoted D in Table 1, is depicted in Fig. 2 c).

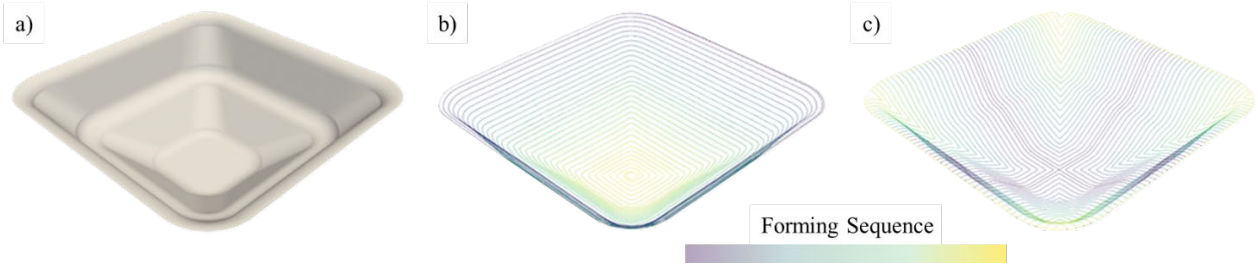

Fig. 2. a) Geometry D5 with b) spiral toolpaths "S" and c) draping toolpaths "D".

As the draping toolpaths are associated with high forming forces, especially in the deepest points of the shape, the step depth is limited, and a large number of intermediate shapes would be required. Therefore, as visible in Table 1, the draping toolpath strategy D was used only for the second-to-last intermediate shape, while all other intermediate shapes were formed with the spiral toolpath S. The toolpath of the last intermediate shape was repeated after deactivating the heating, so that a certain consolidation force was applied during cooling of the FRTP. After forming was finished and the oven temperature was below 40 °C, the layup was removed from the setup, declamped, and the formed part was separated from the metal and PTFE sheets.

Results

All geometries were successfully processed by the digital process chain, generating toolpaths for each intermediate shape and post-processing them to executable code for both robots. The forming process could be finished for all parts but D2-L, the cone with varying wall angle scaled to the biggest possible size in the current setup. In this case, the front steel sheet failed by tearing at a depth of 60 mm, towards the end of forming the second intermediate shape, as shown in Fig. 5 b).

The times for preparing the layup, heating, forming, cooling, and dismantling accumulated to approximately 3 hours for size S geometries, 4.5 hours for the size M geometry, and would have been approximately 10 hours for the size L geometry. The formed parts were analyzed qualitatively regarding possible wrinkling, tearing, or surface defects in the organosheets. Furthermore, a GOM ATOS 3D scanner was used to capture 3D scans of the formed parts, which were then compared to the target geometry by calculating maximum deviations after iterative closest point matching. Finally, a cross-section of part D1-S was prepared and analyzed under an optical microscope, comparing it to virgin material.

Qualitative Analysis.

The results of the demonstrator parts are shown in Fig. 3 and Fig. 5. It can be seen that all small and medium-sized geometries were successfully manufactured, including the non-rotationally symmetrical (D3, D4, D5) and off-center (D3) geometries, the comparably high wall angles up to 60° (D2, D5), and small corner radii of 12 mm (D5). No wrinkling can be observed in the woven fabric in the formed areas, indicating successful fabric draping with visible shear introduced. The coverage of the surface with matrix appears relatively uniform, also in flat areas such as the tips of the cone D1, see Fig. 4, and the pyramid D5. The typical forming defects matrix migration and accumulation, as well as exposed fibers or dry spots, indicating deconsolidation, could largely be avoided. In contrast, the remaining areas of the organosheets surrounding the formed geometry, which would be

trimmed in a postprocessing step, show slight fabric wrinkling, uneven matrix distribution, matrix flaking, and possible dry spots, highlighted as C in Fig. 4. This is due to the fact that they did not experience any tool passes and therefore also no consolidation force from the tool pressure. However, local surface defects can also be observed in the formed areas due to wrinkling of the PTFE foils, which led to imprints in the matrix of the composite, see detail B in Fig. 4. Moreover, particularly the flat tips of the cones D1-S and D2-M show slight grooves of a characteristic spiral shape, corresponding to the tool paths, see detail A in Fig. 4.

In the largest part, D2-L, which could not be formed to the final shape, significant fabric wrinkling can be observed in Fig. 5 a). This is particularly visible in the diagonals of the sheet, where most shear would be necessary. These wrinkles are likely to be attributed to the absence of a drape-aware toolpath, as the experiment had to be terminated before the third intermediate shape, which would have been formed with the draping strategy. Moreover, the comparably large deformations necessary in each intermediate shape, combined with the larger size of the metal sheets, led to a high global deformation and a separation of the metal sheets, leaving room for wrinkles.

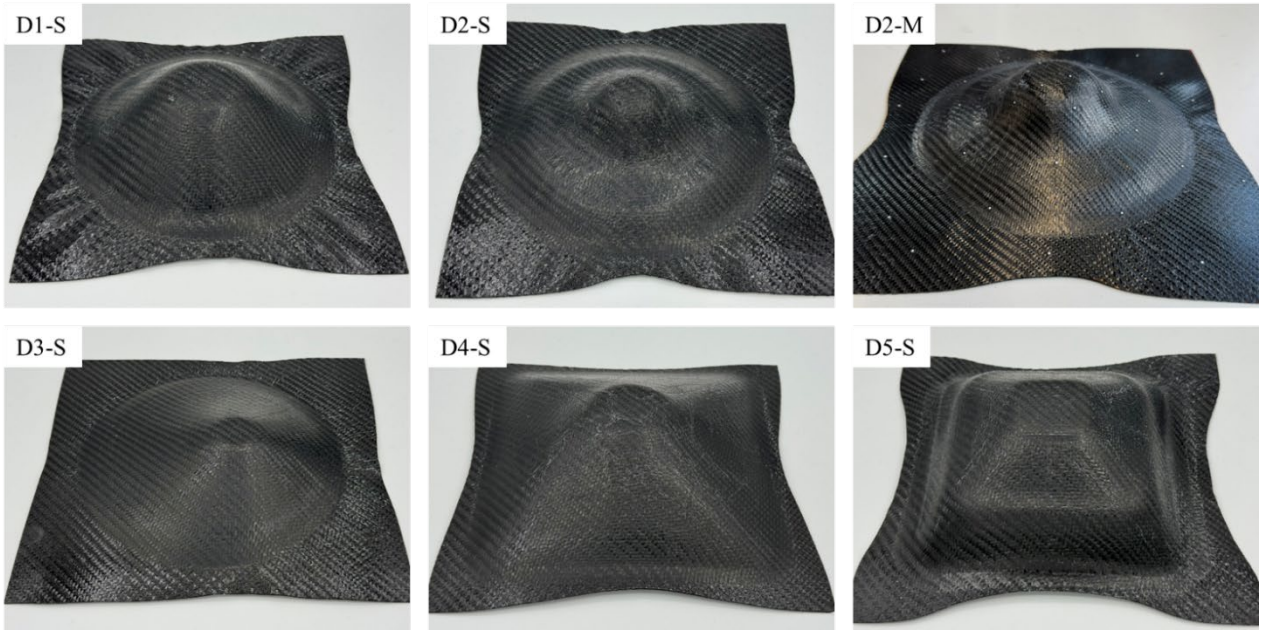

Fig. 3. Successfully formed demonstrator parts D1-D5 in sizes S and M.

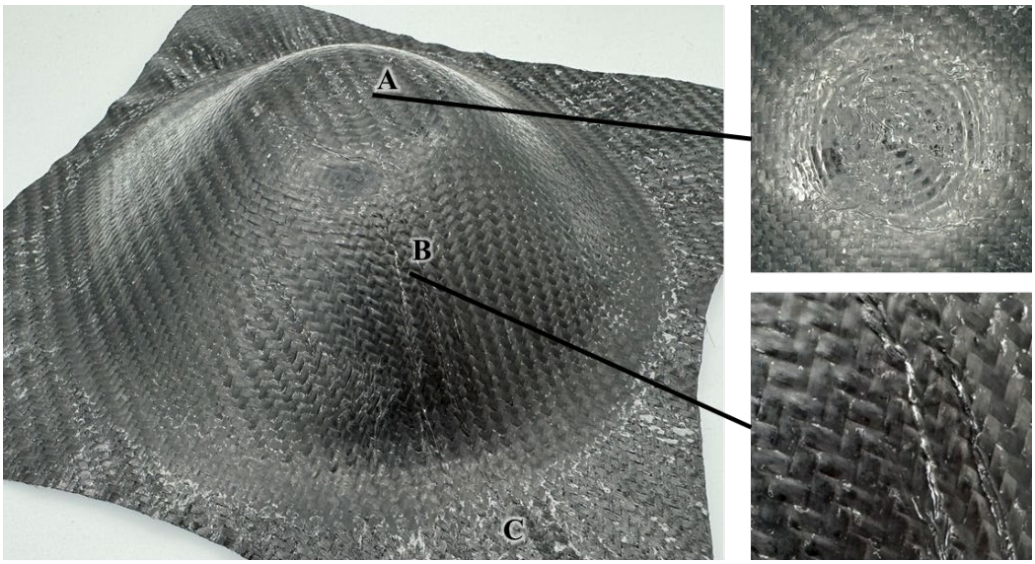

Fig. 4. Formed cone D1-S with generally satisfactory surface quality, but grooves of the tool in the tip (detail A), and imprints of wrinkles of PTFE foil in the matrix (detail B). The surrounding area, which was not formed, shows signs of deconsolidation and wrinkles (C).

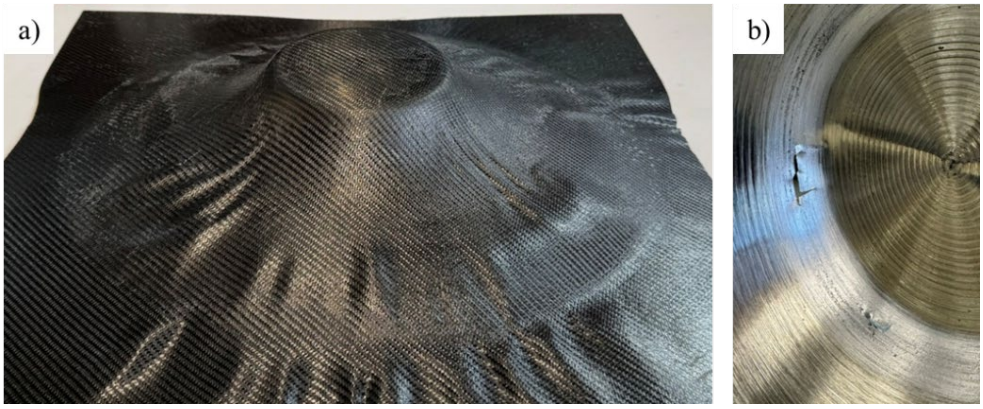

Fig. 5. a) Part D2 in size L, not successfully formed to completion, b) tears in the steel sheet leading to the abortion of the forming process during forming D2-L.

Geometric Accuracy.

The 3D-scanned surfaces of the successfully formed geometries are shown in Fig. 6, with the color scale indicating the signed distance to the target surfaces. The majority of the surface areas lie within a tolerance of ±1 mm. Underforming, indicated by negative values and blue color, appears mostly around the tips of the geometries and along the edges at the transitions between different wall angles in geometries D2 and D5. The corresponding maximum deviation is in a range of 1.55 to 1.82 mm for all geometries except the cones with varying wall angles D2, standing out with a maximum deviation of 2.71 and 2.84 mm at the tip. Meanwhile, a global bending-induced deformation of the sheet layup caused bulging around the base region, leading to overforming near the flange-wall transition, which is indicated by positive values and red color. It is particularly prominent in parts D5 and D2-M, with maximum deviations of 3.35 mm and 2.49 mm, respectively. In the asymmetrical part D3, this effect is pronounced on the side with a higher wall angle. Comparing the two D2 sizes, size M shows slightly larger inaccuracies than size S, with the extent of overforming particularly pronounced in the larger part.

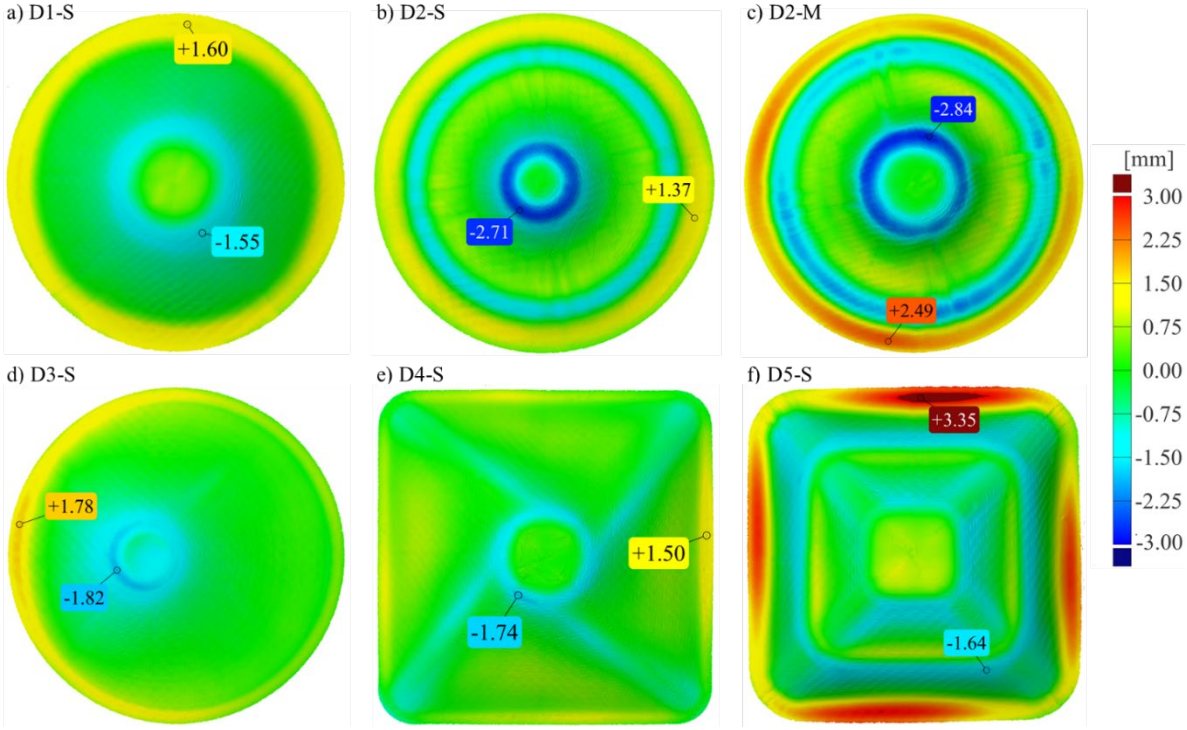

Fig. 6. 3D Scans of the formed geometries, colors indicating the signed distance to the target shapes; a) cone, b) cone with varying wall angle in size S and c) size M, d) cone with eccentric tip, e) square pyramid with twisted circular tip, f) square pyramid with varying wall angle.

Overall, with maximum absolute geometric deviations between 1.6 and 3.35 mm, the geometric accuracy is comparable to that of typical metal DSIF [19–21]. For example, in a recent benchmark study, underforming in critical areas of a complex part was in the range of 1.7 to 3.2 mm, and overforming in the base-wall transition at a maximum of 4 mm [21]. It should be noted that no compensation strategies for machine stiffness or springback have been employed to date. As reported by Konka et al. [20], maximum deviations of a cone could be reduced from 2.2 mm to 1 mm by employing sheet springback and machine stiffness compensation.

Internal Part Quality.

To evaluate the internal part quality and consolidation state, a micrograph of the cross-section of part D1-S was compared with the virgin, pre-consolidated starting material. As visible in Fig. 7, the virgin material shows a homogenous and flat surface covered by matrix material, but internal cracks and voids. As a result of the forming process, the consolidation state of the material was increased, and a reduction in void content was observed. However, as also explained in the qualitative analysis, the surface smoothness was reduced.

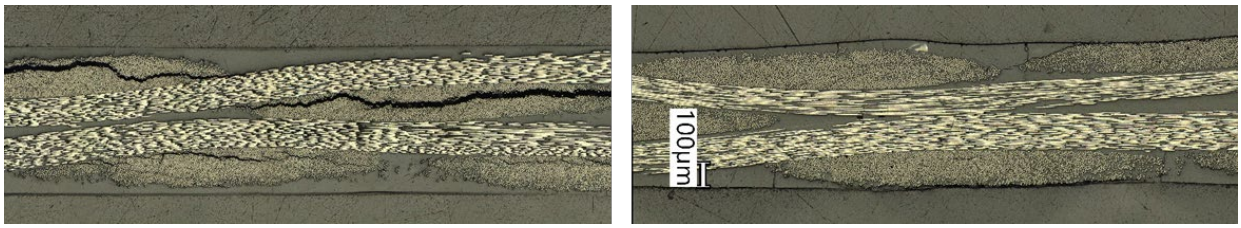

Fig. 7. Micrographs of cross-sections of the virgin material (left) and the formed part D1-S (right).

Conclusion

The experimental results demonstrate the capability of the previously developed hot DSIF setup, digital process chain, and processing strategy to manufacture geometrically diverse parts. Five distinct geometries with individual challenges, including asymmetries, varying wall angles up to 60°, depths up to 50 mm, and corner radii as low as 12 mm, were successfully produced. Most importantly, sufficient shear could be introduced in the fabric to enable wrinkle-free results. Therefore, the forming strategy relying on multiple intermediate shapes, combining classical spiraling and drape-aware toolpaths, proved effective in all of these cases. The pressure applied by the tools during the cooling of the part aided in achieving satisfactory consolidation of the composite material, as evidenced by comparing the formed and peripheral areas of the parts. To further increase the surface quality of the final part, a smaller path distance could be used in the last intermediate shapes. Furthermore, using a separator material with higher strain and a reduced tendency to crease could avoid the matrix imprints currently caused by wrinkles in the PTFE sheets.

3D scans show satisfactory overall geometric accuracy, with maximum deviations arising from underforming at the tip edges and from global deformation at the transition from the base plane to the wall. A higher wall angle and a larger geometry increase this effect. Toolpath compensation algorithms taking into account the elastic springback of the metal sheets as well as the machine stiffness could aid in increasing the geometric accuracy further.

While the process is already somewhat scalable, there are currently still limitations regarding the maximum component size that can be manufactured. The failure of the metal dummy sheet during the forming of the largest part highlights the need for a forming strategy that accounts for both metal and organosheet deformation mechanisms. Further investigations are necessary to enable process optimizations to manufacture parts of larger scale successfully. In addition, forming sheets with higher thicknesses should be investigated to determine process boundaries in this dimension.

Overall, the foundation for a thorough, systematic analysis of relevant process and material parameters is laid by demonstrating the capability of the newly developed DSIF system to produce various parts of different complexity. The experimental results prove the high potential of the novel technology for the flexible manufacturing of FRTP components in prototype, individual part, and

small series production. Further research potential lies in continued optimization of process parameters and in further leveraging the ability to steer the shape evolution by optimizing intermediate shapes and toolpath strategies to achieve even greater process flexibility and part quality.

Acknowledgement

This research was funded by the German Federal Ministry for Economic Affairs and Climate Action under the program LuFo VI-1 iFish, grant number 20Q1917C. We thank the project partners Björn Riecken, Benedikt Kötter, and Christian Keun of CompriseTec GmbH.

References

[1] Estin & Co, Lucintel, JEC Observer, JEC composites magazine. Special issue. (2025).

[2] A. Ogale, C. Weimer, T. Grieser, P. Mitschang, Textile Halbzeuge, in: M. Neitzel, P. Mitschang, U. Breuer (Eds.), Handbuch Verbundwerkstoffe, Carl Hanser Verlag GmbH & Co. KG, München, 2014, pp. 73–93. https://doi.org/10.3139/9783446436978.003.

[3] C. Cherif, The Textile Process Chain and Classification of Textile Semi-finished Products, in: C. Cherif (Ed.), Textile Materials for Lightweight Constructions: Technologies - Methods - Materials - Properties, 1st ed., Springer, Berlin Heidelberg, 2016, pp. 9–35. https://doi.org/10.1007/978-3-662-46341-3_2.

[4] L. Medina, J. Mack, M. Christmann, Imprägnierte Halbzeuge, in: M. Neitzel, P. Mitschang, U. Breuer (Eds.), Handbuch Verbundwerkstoffe, Carl Hanser Verlag GmbH & Co. KG, München, 2014, pp. 135–199. https://doi.org/10.3139/9783446436978.005.

[5] A. Al-Obaidi, A. Kunke, V. Kräusel, Hot single-point incremental forming of glass-fiber-reinforced polymer (PA6GF47) supported by hot air, J. Manuf. Process. 43 (2019) 17–25. https://doi.org/10.1016/j.jmapro.2019.04.036.

[6] J. Jeswiet, Asymmetric Incremental Sheet Forming, AMR 6-8 (2005) 35–58. https://doi.org/10.4028/www.scientific.net/AMR.6-8.35.

[7] R. Malhotra, J. Cao, F. Ren, V. Kiridena, Z. Cedric Xia, N.V. Reddy, Improvement of Geometric Accuracy in Incremental Forming by Using a Squeezing Toolpath Strategy With Two Forming Tools, J. Manuf. Sci. Eng. 133 (2011). https://doi.org/10.1115/1.4005179.

[8] S. Ullah, P. Xu, X. Li, Y. Li, K. Han, D. Li, A Review on Part Geometric Precision Improvement Strategies in Double-Sided Incremental Forming, Metals 12 (2022) 103. https://doi.org/10.3390/met12010103.

[9] T.A. Marques, M.B. Silva, P.A.F. Martins, On the potential of single point incremental forming of sheet polymer parts, Int. J. Adv. Manuf. Technol. 60 (2012) 75–86. https://doi.org/10.1007/s00170-011-3585-y.

[10] H. Zhu, H. Ou, A. Popov, Incremental sheet forming of thermoplastics: a review, Int. J. Adv. Manuf. Technol. 111 (2020) 565–587. https://doi.org/10.1007/s00170-020-06056-5.

[11] C. Hou, X. Su, X. Peng, X. Wu, D. Yang, Thermal-Assisted Single Point Incremental Forming of Jute Fabric Reinforced Poly(lactic acid) Biocomposites, Fibers Polym. 21 (2020) 2373–2379. https://doi.org/10.1007/s12221-020-1016-0.

[12] T.-C. Lim, S. Ramakrishna, Modelling of composite sheet forming: a review, Compos. - A: Appl. Sci. Manuf. 33 (2002) 515–537. https://doi.org/10.1016/S1359-835X(01)00138-5.

[13] K. Jackson, J. Allwood, The mechanics of incremental sheet forming, J. Mater. Process. Technol. 209 (2009) 1158–1174. https://doi.org/10.1016/j.jmatprotec.2008.03.025.

[14] J.-E. Rath, T. Schüppstuhl, Tool path strategies for single point incremental forming of fiber-reinforced thermoplastic sheets, in: Material Forming: ESAFORM 2024, Materials Research Forum LLC, 2024, pp. 641–650. https://doi.org/10.21741/9781644903131-71.

[15] R. Emami, M.J. Mirnia, M. Elyasi, A. Zolfaghari, An experimental investigation into single point incremental forming of glass fiber-reinforced polyamide sheet with different fiber orientations and volume fractions at elevated temperatures, J. Thermoplast. Compos. Mater. 36 (2022) 1893-1917. https://doi.org/10.1177/08927057221074266.

[16] S.M. Mirnia Kalaei, M. Razbin, M. Emami, M.R. Gholami, M. Salehian, F.R. Biglari, Analysis of single-point warm incremental forming for glass fiber-reinforced polyamide 6 sheets: Experimentation and simulation, J. Thermoplast. Compos. Mater. https://doi.org/10.1177/08927057241255884.

[17] G. Ambrogio, F. Borda, R. Conte, L. Filice, F. Gagliardi, Processing of sheets made of long fibers reinforced plastics by SPIF, in: Material Forming: ESAFORM 2024, Materials Research Forum LLC, 2024, pp. 1536–1543. https://doi.org/10.21741/9781644903131-170.

[18] D. Nettig, J.-E. Rath, T. Schüppstuhl, J. Frank, B. Riecken, C.-A. Keun, Hot double sided incremental forming of continuous fiber reinforced thermoplastics: Process analysis and system design, in: Material Forming: ESAFORM 2025, Materials Research Forum LLC, 2025, pp. 1267–1276. https://doi.org/10.21741/9781644903599-138.

[19] S. Ullah, X. Li, P. Xu, Y. Li, K. Han, D. Li, A toolpath strategy for improving geometric accuracy in double-sided incremental sheet forming, CJA 36 (2023) 468–479. https://doi.org/10.1016/j.cja.2021.12.002.

[20] P. Konka, R. Lingam, U.A. Singh, C. Shivaprasad, N.V. Reddy, Enhancement of accuracy in double sided incremental forming by compensating tool path for machine tool errors, Int. J. Adv. Manuf. Technol. 111 (2020) 1187–1199. https://doi.org/10.1007/s00170-020-06149-1.

[21] M. Vanhulst, Y. Lee, D. Steinfels, T. Bremen, K. Perzyński, H. Vanhove, G. Ambrogio, R.-E. Breaz, G. Buffa, R. Conte, L. de Napoli, L. Fratini, X.T. Da Fu, F. Gagliardi, M. Gralha, P. Kang, Ł. Kuczek, A.S. Kumar, A. Kunke, A. Leonhardt, Y. Li, Z. Li, R. Licari, H. Long, D.W.W. Low, S.-G. Racz, P. Scholz, M.B. Silva, S. Song, D. Weise, K. Żaba, H. Zhu, D. Bailly, M. Banu, L. Madej, J.R. Duflou, ESAFORM benchmark 2024: study on the geometric accuracy of a complex shape with single point incremental forming, Int. J. Mater. Form. 18 (2025). https://doi.org/10.1007/s12289-025-01928-1.